A Position-Sensitive Ionization Chamber for Thermal Neutrons

B. Yu, G. J. Mahler, N. A. Schaknowski, and G. C. Smith

***Abstract*—A position-sensitive neutron detector based on ^{3}He is being developed for a national crystal backscattering spectrometer (CBS) at a pulsed neutron source. It comprises a single gas volume, of constant depth, in the form of an annulus that is also part of a truncated cone. Charge from each event is collected on one or two anode strips, out of a total 336 around the annulus, yielding an angular resolution of about 1°. Low-noise signal processing, in the form of a monolithic preamplifier/shaping amplifier connected to each anode strip, provides electronic noise that is small enough to permit detector operation in ionization mode. In addition, the segmented anodes ensure near complete induced charge collection. This new detector therefore has significant advantages over previous detectors used in CBS instruments, which primarily consisted of arrays of individual ^{3}He filled cylindrical counters with dead regions and nonuniform detection efficiency. The optimization of gas mixture/pressure, drift field, and shaping time is significant in achieving successful performance in the new detector.**

***Index Terms*—Ionization chambers, neutron detectors, position sensitive particle detectors.**

I. Introduction

COLD neutrons can be used to provide unique information on the structure and dynamics of condensed matter systems using a crystal backscattering spectrometer (CBS). A proposal for a state-of-the-art CBS at the Spallation Neutron Source (SNS) is being made. The Rutherford Appleton Laboratory presently has the most advanced CBS at its spallation neutron source.[1] We are developing a new position-sensitive ionization chamber for the detection of neutrons with energies in the range of 6–20 Å. Currently, the most widely used detectors for this purpose are arrays of individual ^{3}He tubes. In comparison, this new detector provides higher detection efficiency and better position resolution. To simplify the detector construction, it is operated in ionization mode instead of the more conventional multiwire proportional chamber (MWPC) multiplication mode [1]. This approach could be adapted to a range of neutron scattering techniques in which linear position encoding in a single gas volume could improve an instrument's performance.

II. Principles of Operation

Thermal neutrons convert in ^{3}He through the following reaction:

$$^3\mathrm{He} + n \rightarrow {}^3\mathrm{H} + p + 764\ \mathrm{keV}. \tag{1}$$

Manuscript received November 5, 2000; revised February 9, 2001. This work was supported by the U.S. Department of Energy under Contract DE-AC02-98CH10886.

The authors are with Brookhaven National Laboratory, Upton, NY 11973 USA.

Publisher Item Identifier S 0018-9499(01)04762-1.

[1]See ISIS, http://www.isis.rl.ac.uk/molecularspectroscopy/iris/index.htm.

The products, a 191-keV triton and a 573-keV proton, are emitted in opposite directions, forming a trail of electrons and positive ions. The total number of electron–ion pairs created in this process is about 25 000 (4 fC). The ionization centroid of the two particle tracks is displaced from the neutron interaction position because the proton is more heavily ionizing than the triton and has a larger range. The proton range varies inversely with the gas density. Since ^{3}He is not very efficient in stopping the projectiles, an additional gas is needed to provide stopping power for the proton and triton in order to achieve resolution in the millimeter range. Propane is chosen because of its high stopping power and low sensitivity to gamma radiation. The proton range is about 1 mm in 4 atm of propane.

The detector operates as an ionization chamber with an array of anode strips in a parallel plate drift field. The electrons and ions created by the energetic proton and triton projectiles drift toward the anode and cathode planes, respectively, inducing characteristic charge current in the anode strips.

By Ramo's theorem [2], the amount of charge induced on a given electrode by a point charge Q at (x, y) equals the charge Q times the value of an induction field $U(x, y)$, which is calculated by applying a unit potential on the electrode of interest with all other electrodes grounded. In the case of one strip in a parallel plate geometry, the exact expression for this induction field is [3]

$$U(x,y) = \frac{1}{\pi}\left\{\arctan\left[\tanh\left(\pi\frac{x+a/2}{2d}\right)\cdot\tan\left(\pi\frac{y}{2d}\right)\right] - \arctan\left[\tanh\left(\pi\frac{x-a/2}{2d}\right)\cdot\tan\left(\pi\frac{y}{2d}\right)\right]\right\} \tag{2}$$

where a is the width of the strip and d is the distance between the two parallel plates. Fig. 1 shows a contour plot of the function $U(x, y)$ in the geometry of our detector.

Since the drift field in this geometry is constant, so is the electron drift velocity v_d. The induced current in a strip centered at $(0, d)$ by a point charge Q can be derived from the gradient of $U(x, y)$ along the drift path

$$i(x,y) = -Q\nabla U(x,y)\cdot\vec{v}_d. \tag{3}$$

Because the positive ions created by the primary ionization move at a much lower velocity than that of the electrons, their contribution to the induced charge signal is negligible within the measurement time of this detector.

Fig. 2(a) shows the calculated induced current waveforms from three adjacent strips by a single point charge starting from the origin, moving along the y-axis toward the $n = 0$ strip. Initially, the point charge induces small, nearly equal amount of

0018–9499/01$10.00 © 2001 IEEE

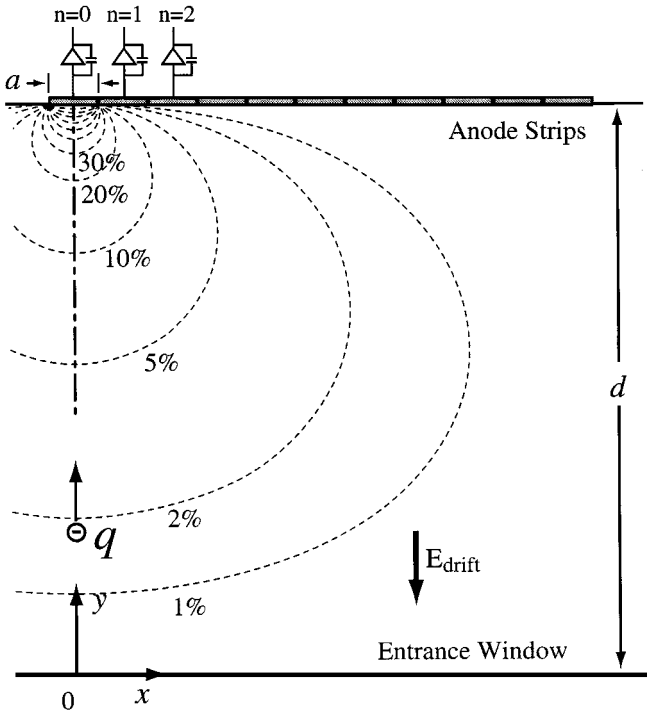

Fig. 1. The contour plot of the induction field (a.k.a. weighting field) for this ionization chamber geometry. $d = 2$ cm and $a = 1.74$ mm are used throughout this paper.

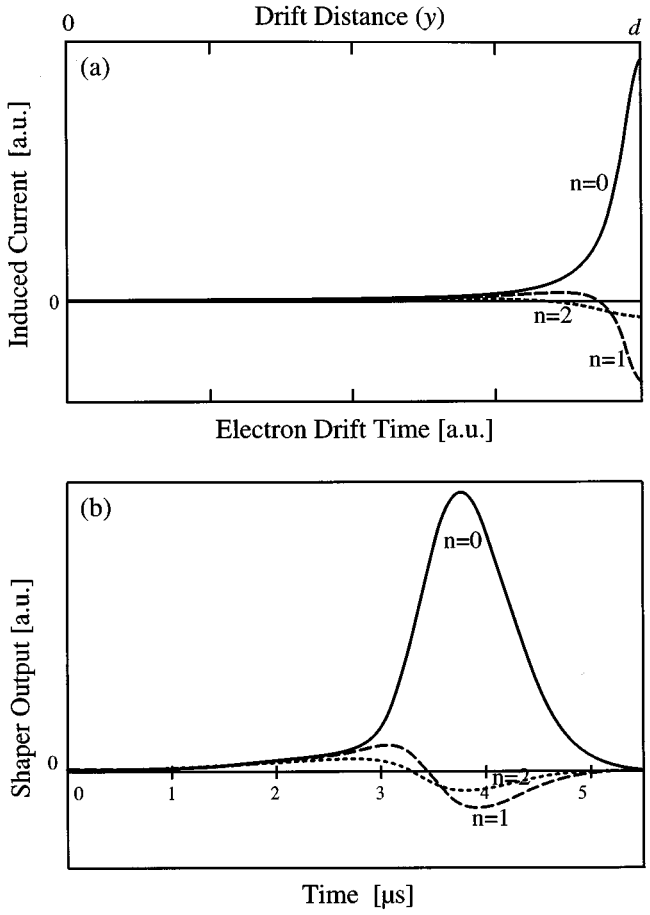

Fig. 2. (a) Induced current waveform on the three adjacent strips from a point charge starting from (0, 0) moving toward (0, d). (b) Simulated shaper output for the current waveforms shown in (a). The total electron drift time used here is about 2.5 μs.

current on all three strips. As the charge moves to a distance a few times the strip width from the strips, the induced current increases rapidly for the collecting strip and reverses polarity for the noncollecting strips. The net charge on a noncollecting electrode is always negative. Clearly, most of the signal current on the strip electrodes is induced when the point charge is very close to the strips. If the starting points of all ionization events can be contained near the entrance side of the drift volume, the resolution of the pulse-height spectrum is greatly improved. This can be achieved by making the absorption depth of the incoming radiation shorter than the drift depth.

Convolving the induced current waveform with the shaping amplifier's impulse response function gives the shaper output waveform. Fig. 2(b) shows the calculated output waveform with a 1.2-μs peaking time unipolar shaping amplifier [4]. Even though the net charge induced on a noncollecting electrode is always negative, its waveform may exhibit a small positive lobe due to the small positive current at the early stage of the drift.

In the final detector, the output of the preamp shaper is not digitized but is sent to a set of discriminators in the data acquisition system [5]. All strips in the detector are scanned at about 1-μs intervals to obtain a neutron hit pattern. The position of a neutron is derived from the position of the strip whose signal exceeds the threshold. For those events in which more than one strip registers a hit because of charge sharing, the center of gravity of all hit strips is used as the neutron position.

III. Monte Carlo Simulations

A Monte Carlo simulation program has been developed to study the performance of the detector in ionization mode and to optimize its operating parameters. The program takes into account many aspects of the physical processes in the detector, such as the proton/triton tracks, wall effect, electron lifetime, front-end electronics impulse response, etc. The key parameters are the drift distance and the pressures of ^{3}He and propane. For example, a high ^{3}He pressure is preferred for high neutron absorption efficiency; but it also makes wall effects more prominent for low-energy neutron events, because they are absorbed too close to the entrance window. Increasing the propane pressure will reduce the proton/triton track lengths, alleviating the wall effect to some extent; but then high pressure will not only slow down the electron drift speed but also cause complications in the mechanical design of the pressure vessel.

One of the requirements from the experimenters is high detection efficiency in the neutron energy range of interest. Fig. 3 shows the number of strips whose signals exceed the discriminator threshold as a function of the discriminator level at a propane pressure of 4 atm. Clearly, an efficiency of better than 95% can be achieved by choosing a discriminator level between 20% and 40% of the full signal. Threshold level below 20% should be avoided because of the electronic noise ($\sim$3% rms of the full signal in our test setup), which is not included in this diagram, as well as the small positive overshoots from noncollecting strips [Fig. 2(b)]. Since the position decoding is done

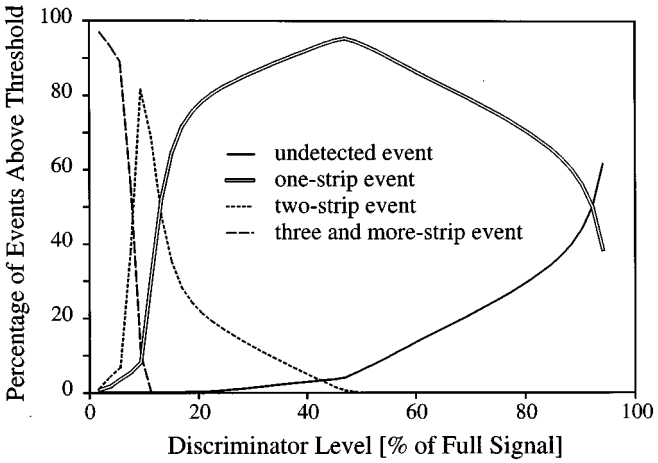

Fig. 3. Computer simulation results showing the percentage of events above threshold as a function of the discriminator level. The events are grouped into four catagories, depending on the number of strips above the discriminator threshold. Propane pressure used is 4 atm. Electronic noise is not included.

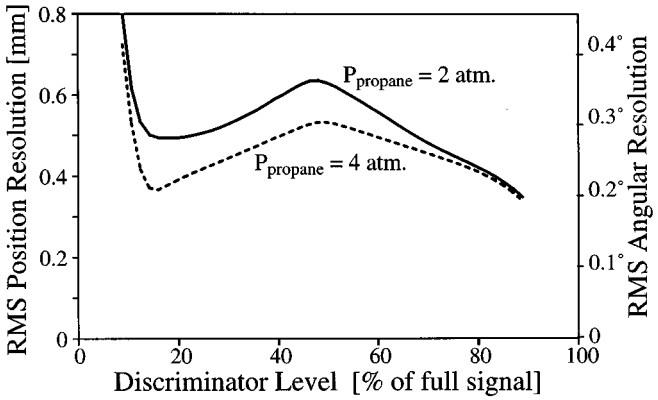

Fig. 4. Computer simulation results showing the detector's rms position resolution as a function of the discriminator level at propane pressure of 4 and 2 atm.

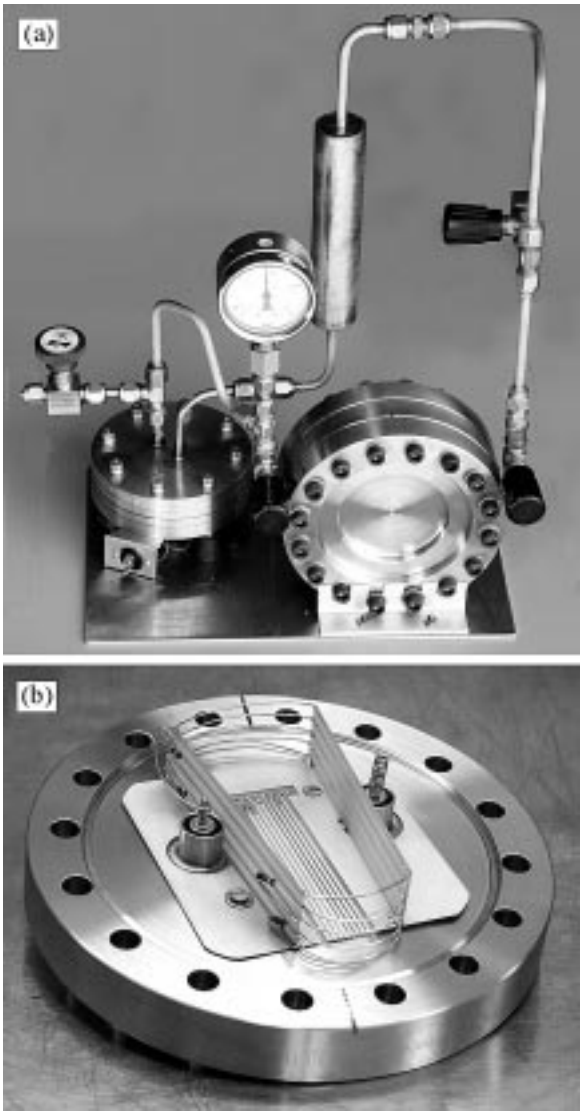

Fig. 5. Photograph of (a) a small test chamber and (b) the inner electrode structure. The anode strips lay flat against the conflat flange. A set of field shaping electrodes surrounds the drift volume. Not shown is the cathode window, which is a sheet of copper clad Kapton glued onto the facing flange.

only by discriminators, the neutron position for each event is calculated from the geometric center of the anode strips whose signal crosses the threshold.

Computer-simulated position resolution as a function of the discriminator level at propane pressures of 4 and 2 bar is shown in Fig. 4. The strip pitch is 1.74 mm. The peak values at the midthreshold range coincide with the rms contributions of the strip width and the proton-triton ranges. At a lower discriminator level, one or more strips are used in the center of gravity calculation, resulting in better position determination. At even lower thresholds (<15%), electronic noise degrades the resolution. It is interesting to note that at high discriminator threshold levels (>50%), the position resolution is better than the nominal statistical limit. It is believed that at high thresholds, the events that cross the threshold no longer have the usually uniform spatial distribution. However, this does not have much practical significance because the efficiency is very low.

Gamma-ray background is not included in the simulation. The gas mixture chosen in this work has very low sensitivity to gamma rays. Results from our MWPCs [6] using similar gas mixture have shown that the deposited energy from gamma rays is well below 20% of that from the neutrons. For a real detector, the optimal discriminator threshold setting should probably be set between 20–40% of full signal to maintain good detection efficiency as well as noise and gamma-ray immunity.

IV. Test Chamber Results

A small test chamber has been built to evaluate the feasibility of the ionization mode of operation. The chamber is constructed from three stainless-steel conflat flanges. Fig. 5 shows a photograph of the test chamber and its inner electrode arrangement. It has a drift depth of 2 cm and four sensing strips at a 1.74-mm pitch. A field shaping grid is placed around the active drift volume. A gas mixture of 4 atm of ^{3}He and 4 atm of propane was used. The front-end electronics chosen for this work is a high-performance CMOS application-specific integrated circuit (ASIC) [4]. Originally designed for CZT detectors, this ASIC has 16 channels of preamps and shapers on each chip. It has a programmable gain range of 30–200 mV/fC and a peaking time from 0.6 to 4 μs. The test chamber was placed

in front of an Am-Be neutron source encased in paraffin wax. This achieved uniform irradiation of the chamber with a flux of thermal neutrons.

A propane pressure of 4 atm limits the proton range to around 1 mm. A large fraction of events induce signal on only a single strip. At 4 atm of ^{3}He, more than 90% of neutrons in the 6–20 Å energy range are absorbed in the top half of the drift field. Since the electrons are traversing most of the drift field, they induce nearly all the charge from the collecting strip. Pulse-height histograms of a single strip over a range of drift fields and shaping times are shown in Fig. 6. The decrease in peak height at low drift fields or short shaping times is due to the ballistic deficit in the shaping amplifier: the electron drift time is much longer than the shaping time. These measurements indicate that a shaping time above 1 μs is adequate to collect most of the charge at a drift field of 2.5 kV/cm.

The events in the midsection of the pulse-height spectra are those that share charge between two adjacent strips. It is more evident in a plot of the induced signal correlation between two neighboring strips. Fig. 7 shows a Monte Carlo simulation and an experimental result of a two-dimensional (2-D) histogram of the induced charge on two adjacent anode strips n and $n+1$. A projection onto either axis will give the one-dimensional induced charge pulse-height spectra, shown in Fig. 6. Events in region 1 are those that have shared charge between strip n and $n+1$. Events in region 2 are mostly those with shared charge between strip $n+1$ and $n+2$. Similarly, events in region 3 correspond to charge sharing between $n-1$ and n. The large concentration of events near the origin is due to events that arrive on more distant strips [the positive lobes in the noncollecting strip waveform, Fig. 2(b)]. A set of hybrid preamplifiers and 1-μs delay line amplifiers was used to obtain this 2-D histogram—the ASIC does not have enough gain to get a complete picture due to the limitations in our pulse-height analyzer.

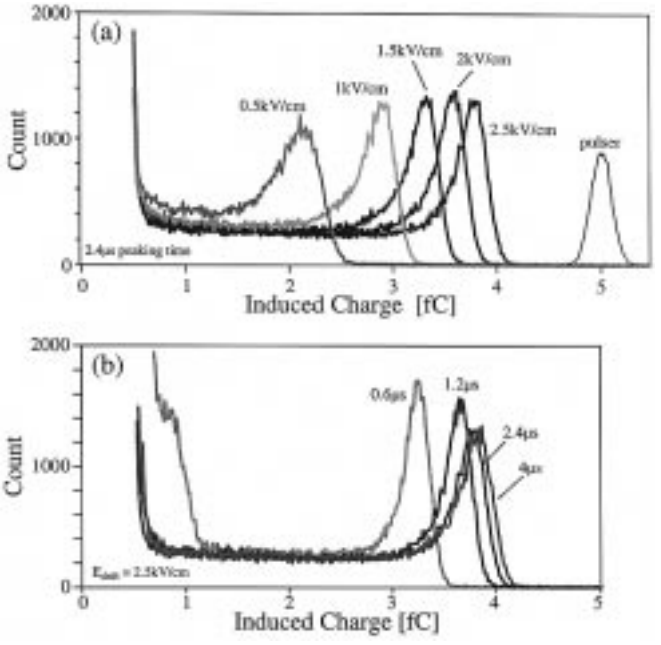

Fig. 6. (a) Induced charge spectra for different magnitudes of drift field, with detector operated in ionization mode. (b) Induced charge spectra at different shaper peaking time.

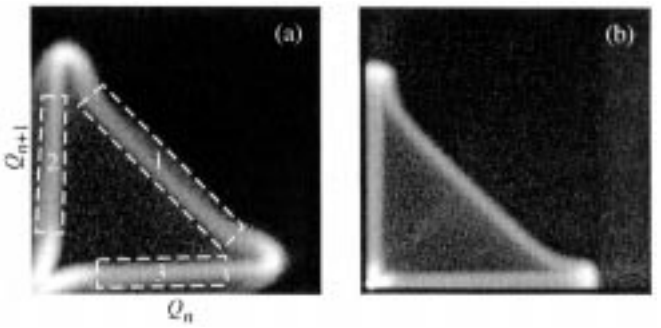

Fig. 7. Two-dimensional histograms of the induced charge on two adjacent anode strips n and $n+1$. (a) Computer simulation and (b) test chamber results. The intensity scale is logarithmic.

V. Construction of the Final Detector

Fig. 8 shows a cross-section and picture of the final detector, which is presently under construction. It is in the form of a truncated cone, with a 20-cm diameter at the midplane and an active window height of 6 cm. A uniform drift distance of 2 cm is maintained between the entrance window (a sheet of copper-clad Kapton provides the bias voltage) and the anode plane (a Kapton sheet with 336 vertical copper strips). The strips are spaced at 1° intervals around the cone, covering 336°. Each strip is connected through multipin high-pressure feedthroughs to its own preamp and shaper circuits [4] outside the pressure vessel. A new version of the ASIC optimized for this detector's input capacitance ($\sim$10 pF) will be developed. Following each shaper is a buffer amplifier, which provides differential output through twisted pair cables to the data acquisition system. The "top hat" of the pressure vessel, shown in Fig. 8, is machined from a block of 7075 aluminum alloy. It has an entrance window thickness of only 1.4 mm. The pressure vessel is rated at 10.5 atm. An electromagnetic diaphragm pump and purifier will be attached to the sealed detector to constantly remove any impurities in the gas. This approach has been used because existing two-dimensional detectors based on the same design philosophy [1] have operated reliably over several years in high-flux neutron experiments. In the meantime, we are investigating the use of CF_4, which has a higher electron drift velocity compared to propane. The performance of the final detector will be reported at a later time.

The operation of gas-filled neutron detectors in ionization mode provides a robust and stable instrument which, when designed with a single gas volume as used in this project, offers a solution that is cost-competitive and more efficient compared with existing instruments using proportional tubes. With the increasing availability of low noise monolithic electronics, it is likely that this type of instrument will find greater use in a wide range of future neutron experiments.

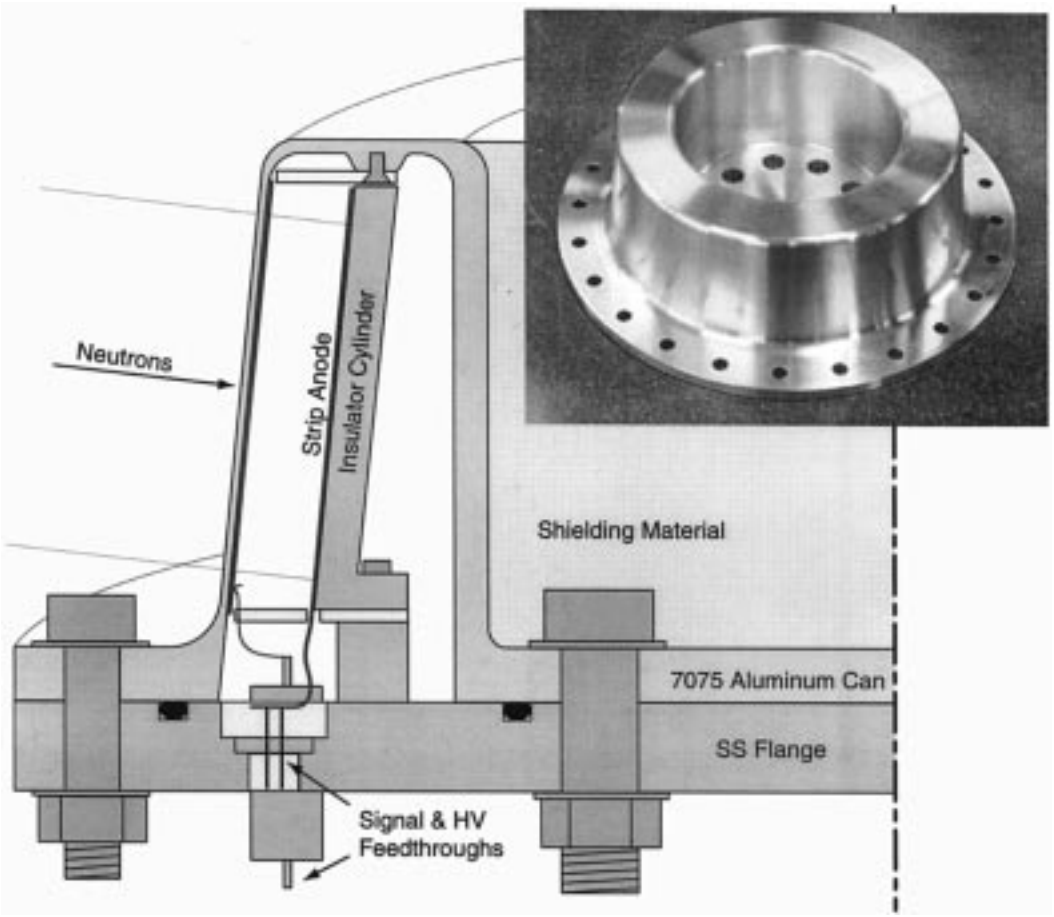

Fig. 8. Cross section (half-view) of the neutron detector for crystal backscattering spectrometer—it provides angular resolution of about 1°. Neutrons are diffracted from a circular array of crystals (not shown) that surround the detector. The upper right photo is the "top hat" of the pressure vessel.

ACKNOWLEDGMENT

The authors wish to thank Dr. J. Larese, BNL, for calling attention to the Crystal Backscattering Spectrometer application. They acknowledge support and encouragement from both him and Dr. S. Gushue during this detector development.

REFERENCES

[1] V. Radeka, N. A. Schaknowski, G. C. Smith, and B. Yu, "High precision thermal neutron detectors," in *Neutron in Biology*, B. Schoenborn and R. Knott, Eds. New York: Plenum, 1996, pp. 57–67.

[2] S. Ramo, "Current induced by electron motion," *Proc. IRE*, vol. 27, pp. 584–585, 1939.

[3] P. Rehak, D. Cline, E. Gatti, C. Heusch, S. Kahn, and B. King *et al.*, "Detector challenges for $\mu^+\mu^-$ colliders in the 10–100 TeV range,", Brookhaven National Laboratory Rep. 67 213.

[4] G. De Geronimo, P. O'Connor, and J. Grosholz, "A generation of CMOS readout ASIC's for CZT detectors," *IEEE Trans. Nucl. Sci.*, vol. 47, pp. 1857–1867, 2000.

[5] C. Rose, "Argonne National Laboratory-based time-of-flight (TOF) VXI module," LANSCE-12, Tech. Note LA-UR-00-1842, available e-mail: crose@lanl.gov.

[6] R. A. Boie, J. Fischer, Y. Inagaki, F. C. Merritt, H. Okuno, and V. Radeka, "Two-dimensional high precision thermal neutron detector," *Nucl. Instrum. Meth.*, pp. 533–545, 1982.